Available online at www.sciencedirect.com
ScienceDirect
Engineering Fracture Mechanics 75 (2008) 986–1004
Engineering Fracture Mechanics
www.elsevier.com/locate/engfracmech

Coupling of the meshfree and finite element methods for determination of the crack tip fields

Y.T. Gu [a,b], L.C. Zhang [b,*]

[a] School of Engineering Systems, Queensland University of Technology, G.P.O. Box 2434, Brisbane, QLD 4001, Australia
[b] School of Aerospace, Mechanical and Mechatronic Engineering, The University of Sydney, NSW 2006, Australia

Received 28 November 2006; received in revised form 3 May 2007; accepted 3 May 2007
Available online 16 May 2007

Abstract

This paper develops a new concurrent simulation technique to couple the meshfree method with the finite element method (FEM) for the analysis of crack tip fields. In the sub-domain around a crack tip, we applied a weak-form based meshfree method using the moving least squares approximation augmented with the enriched basis functions, but in the other sub-domains far away from the crack tip, we employed the finite element method. The transition from the meshfree to the finite element (FE) domains was realized by a transition (or bridge region) that can be discretized by transition particles, which are independent of both the meshfree nodes and the FE nodes. A Lagrange multiplier method was used to ensure the compatibility of displacements and their gradients in the transition region. Numerical examples showed that the present method is very accurate and stable, and has a promising potential for the analyses of more complicated cracking problems, as this numerical technique can take advantages of both the meshfree method and FEM but at the same time can overcome their shortcomings.

Keywords: Crack; Meshfree; Meshless; Finite element method; Concurrent simulation; Fracture mechanics; Numerical analysis

1. Introduction

The finite element method (FEM) is currently a dominant numerical tool in the analysis of fracture mechanics problems, especially for stationary cracks. A large variety of approaches have been developed in the analysis of the field of crack tip by FEM. However, FEM often experiences difficulties in re-meshing and adaptive analysis. In addition, FEM is often difficult (or even impossible) to simulate some problems such as the large deformation problems with severe element distortions, crack growth problems with arbitrary and complex paths which do not coincide with the original element interfaces, and the problems of breakage of material with large number of fragments. Meshfree (or meshless) methods have recently become attractive alternatives for problems in computational mechanics, as they do not require a mesh to discretize the problem

* Corresponding author. Fax: +61 2 93517060.
E-mail address: zhang@aeromech.usyd.edu.au (L.C. Zhang).

0013-7944/$ - see front matter
doi:10.1016/j.engfracmech.2007.05.003

Nomenclature

$\mathbf{a}$	vector of interpolation coefficients, defined in Eq. (2)
$\mathbf{A}$, $\mathbf{B}$	interpolation matrices, defined in Eqs. (7) and (8)
$\mathbf{A}_{(\mathrm{FE})}$, $\mathbf{A}_{(\mathrm{MM})}$	transition matrices for FEM and meshfree method, defined in Eqs. (44) and (45)
$\mathbf{b}$	vector of body force, defined in Eq. (14)
$\mathbf{B}_{(\mathrm{FE})}$, $\mathbf{B}_{(\mathrm{MM})}$	transition matrices for FEM and meshfree method, defined in Eqs. (36) and (38)
$\mathbf{D}$	Matrix of material constants
$\mathbf{f}_{(\mathrm{MM})k}$, $\mathbf{f}_{(\mathrm{MM})k}$	force vectors at a particle k obtained by the FEM and meshfree method, defined in Eqs. (26) and (27)
$\mathbf{F}_{(\mathrm{FE})}$, $\mathbf{F}_{(\mathrm{MM})}$	force vectors for FEM and meshfree method, defined in Eqs. (23) and (24)
g	generalized displacement of a transition particle, defined in Eq. (28)
$g_{(x)}$	generalized derivative of a transition particle, defined in Eq. (41)
K_{I}, K_{II}, K_{III}	stress intensity factors for mode-I, mode-II, and mode-III
$\mathbf{K}_{(\mathrm{FE})}$, $\mathbf{K}_{(\mathrm{MM})}$	stiffness matrices for FEM and meshfree method, defined in Eqs. (21) and (22)
$\mathbf{n}$	vector of the unit outward normal, defined in Eq. (14)
N	FEM shape function, defined in Eq. (18)
p_j	monomial of polynomial basis functions, defined in Eq. (2)
(R, θ)	cylindrical coordinate, defined in (10)
$\mathbf{u}$	displacement vector, defined in Eq. (14)
$\mathbf{u}_{(\mathrm{MM})k}$, $\mathbf{u}_{(\mathrm{MM})k}$	displacement vectors at a particle k obtained by the FEM and meshfree method, defined in Eqs. (26) and (27)
$\bar{\mathbf{u}}$, $\bar{\mathbf{t}}$	prescribed boundary displacement and traction, defined in Eqs. (15) and (16)
w	weight function, defined in Eq. (3)
$\mathbf{x}$	coordinate vector
Γ	global boundary
ϕ	shape function, defined in Eq. (6)
Φ	shape function matrix, defined in Eq. (29)
Π	functional
Γ_{u}, Γ_{t}	boundaries for displacement and traction boundary conditions, defined in Eqs. (15) and (16)
ε, σ	vectors of strain and stress, defined in Eqs. (17) and (14)
λ, γ	Lagrange multiplier, defined in Eqs. (34) and (42)
Λ, Ψ	selected interpolation for λ and γ, defined in Eqs. (34) and (44)
Ω	problem domain
Ω_{s}	local domain to construct meshfree shape functions

domain, and the approximate solution is constructed entirely by a set of scattered nodes. Some meshfree methods have been developed and achieved remarkable progress, such as the smooth particle hydrodynamics (SPH) [1], the element-free Galerkin (EFG) method [2], the reproducing kernel particle method (RKPM) [3,4], the meshfree local Petrov–Galerkin (MLPG) method [5–7], and the local radial point interpolation method (LRPIM) [8–11]. The principal attraction of the meshfree methods is their capacity in dealing with moving boundaries and discontinuities, such as phase changes and crack propagations, and their ease in using the enriched basis functions based on the asymptotic displacement fields near the crack tip [12].

However, the meshfree method usually has worse computational efficiency than FEM, because more computational cost is required in the meshfree interpolation and numerical integrations [13]. Although the burden of the computational cost is being alleviated due to the development of computer technologies, to improve the computational efficiency is still a key factor for the simulations of many practical problems, for example, the three-dimensional dynamic crack problem, etc. Some strategies have been developed for the alleviation of the above-mentioned problems, but how to improve the efficiency of the meshfree methods is still an open problem. Coupling the meshfree methods with FEM can be a possible solution.

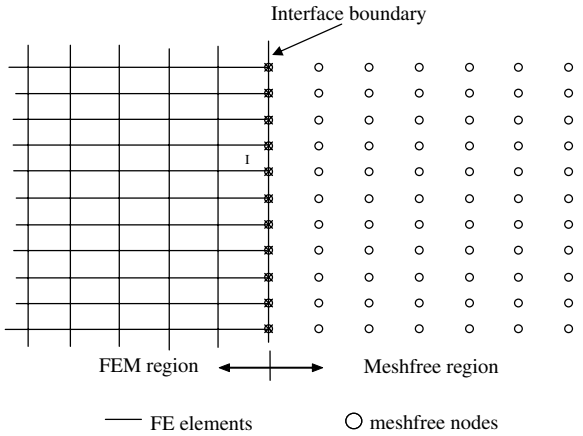

Fig. 1. The coupled techniques using the interface boundary.

In the analysis of crack problems, we can find that a crack region usually occupies only a small part in the whole problem domain. It is desirable and beneficial to combine the meshfree methods with FEM in order to exploit their advantages while evading their disadvantages. In the coupling, the meshfree method can be used only in a sub-domain including the crack and its unique advantages are beneficial to get accurate and stable results. FEM can be employed in the remaining parts of the domains and its good computational efficiency can save much computational cost. In some previous research on the coupling of EFG/FEM/boundary element method (BEM), MLPG/FEM/BEM, and so on [14–18], the major difficulty was how to satisfy the compatibility conditions on the interface between the domains of two methods [19], even with interface element methods and methods based on extension of weak forms. In these techniques, a common interface boundary (e.g., a curve for a two-dimensional problem, as shown in Fig. 1) is often used between FEM domain, $\Omega_{(\mathrm{FE})}$, and the meshfree domain, $\Omega_{(\mathrm{MM})}$. The meshfree nodes and the FEM nodes along this interface boundary coincide with each other, and are dependent on each other. In addition, it is difficult to ensure the high-order compatibility using the interface boundary [19].

This paper aims to develop an advanced coupled meshfree method (MM)/FEM for crack problems. The problem domain is divided into several sub-domains: one domain including the crack is simulated by the meshfree method, the other sub-domains are simulated by FEM, and these two parts are connected by a transition region (or bridge region). A new transition algorithm is proposed to ensure a smooth transition between the meshfree and FEM sub-domains. To simplify the numerical integrations, several layers of transition particles are inserted in the transition region and the Lagrange multipliers method is used to ensure the compatibility conditions. The meshfree shape functions augmented with the enriched basis functions to predict the singular stress fields near a crack tip are constructed. Around the crack, the relay model [20] is used for the nodal selection and computing the influence of nodes. Several numerical examples of crack problems are presented to demonstrate the validity and efficiency of the new coupled method.

2. Enriched moving least squares approximation

To approximate a function $u(\mathbf{x})$ in Ω_s, a finite set of $\mathbf{p}(\mathbf{x})$ called basis functions is considered in the space coordinates $\mathbf{x}^{\mathrm{T}} = [x,y]$. The basis functions in two-dimension is given by

$$\mathbf{p}^{\mathrm{T}}(\mathbf{x}) = [1, x, y, x^2, xy, y^2, \ldots] \tag{1}$$

The moving least square approximation (MLSA) interpolant $u^h(x)$ is defined in the domain Ω_S by

$$u^h(\mathbf{x}) = \sum_{j=1}^{m} p_j(\mathbf{x}) a_j(\mathbf{x}) = \mathbf{p}^{\mathrm{T}}(\mathbf{x})\mathbf{a}(\mathbf{x}) \tag{2}$$

where m is the number of basis functions, and the coefficients $a_j(x)$ are also functions of $\mathbf{x}$; $\mathbf{a}(\mathbf{x})$ is obtained at any point $\mathbf{x}$ by minimizing a weighted discrete $\mathbf{L}_2$ norm of:

$$J = \sum_{i=1}^{n} w(\mathbf{x}-\mathbf{x}_i)[\mathbf{p}^{\mathrm{T}}(\mathbf{x}_i)\mathbf{a}(\mathbf{x}) - u_i]^2 \tag{3}$$

where n is the number of nodes in the neighborhood of $\mathbf{x}$ for which the weight function $w(\mathbf{x}-\mathbf{x}_i) \neq 0$, and u_i is the nodal value of u at $\mathbf{x} = \mathbf{x}_i$.

The stationarity of J with respect to $\mathbf{a}(\mathbf{x})$ leads to the following linear relation between $\mathbf{a}(\mathbf{x})$ and $\mathbf{u}$:

$$\mathbf{A}(\mathbf{x})\mathbf{a}(\mathbf{x}) = \mathbf{B}(\mathbf{x})\mathbf{u} \tag{4}$$

Solving $\mathbf{a}(\mathbf{x})$ from Eq. (4) and substituting it into Eq. (2), we have

$$u^h(\mathbf{x}) = \sum_{i=1}^{n} \phi_i(\mathbf{x})u \tag{5}$$

where the MLSA shape function $\phi_i(\mathbf{x})$ is defined by

$$\phi_i(\mathbf{x}) = \sum_{j=1}^{m} p_j(\mathbf{x})(\mathbf{A}^{-1}(\mathbf{x})\mathbf{B}(\mathbf{x}))_{ji} \tag{6}$$

In which $\mathbf{A}(\mathbf{x})$ and $\mathbf{B}(\mathbf{x})$ are the matrices defined by

$$\mathbf{A}(\mathbf{x}) = \sum_{i=1}^{n} w_i(\mathbf{x})\mathbf{p}^{\mathrm{T}}(\mathbf{x}_i), \mathbf{p}(\mathbf{x}_i), \quad \text{where } w_i(\mathbf{x}) = w(\mathbf{x}-\mathbf{x}_i) \tag{7}$$

$$\mathbf{B}(\mathbf{x}) = [w_1(\mathbf{x})\mathbf{p}(\mathbf{x}_1), w_2(\mathbf{x})\mathbf{p}(\mathbf{x}_2), \ldots, w_n(\mathbf{x})\mathbf{p}(\mathbf{x}_n)] \tag{8}$$

It should be mentioned here that the MLSA shape function obtained above does not have the Kronecker delta function properties [13].

In two-dimensional linear elastic fracture mechanics, both mode-I and mode-II crack-tip fields should be considered. For mode-I deformations, the crack-tip stresses have the following formulations [21]

$$\begin{Bmatrix} \sigma_{11} \\ \sigma_{22} \\ \sigma_{12} \end{Bmatrix} = \frac{K_{\mathrm{I}}}{\sqrt{2\pi r}} \cos\frac{\theta}{2} \begin{Bmatrix} 1 - \sin\frac{\theta}{2}\sin\frac{3\theta}{2} \\ 1 + \sin\frac{\theta}{2}\sin\frac{3\theta}{2} \\ \sin\frac{\theta}{2}\sin\frac{3\theta}{2} \end{Bmatrix} \tag{9}$$

For mode-II deformations, the crack-tip stresses are [21]

$$\begin{Bmatrix} \sigma_{11} \\ \sigma_{22} \\ \sigma_{12} \end{Bmatrix} = \frac{K_{\mathrm{II}}}{\sqrt{2\pi r}} \cos\frac{\theta}{2} \begin{Bmatrix} -\sin\frac{\theta}{2}\left(2 + \cos\frac{\theta}{2}\cos\frac{3\theta}{2}\right) \\ \sin\frac{\theta}{2}\cos\frac{\theta}{2}\cos\frac{3\theta}{2} \\ \cos\frac{\theta}{2}\left(1 - \sin\frac{\theta}{2}\sin\frac{3\theta}{2}\right) \end{Bmatrix} \tag{10}$$

where K_{I} and K_{II} are the stress intensity factors for mode-I and mode-II dependent upon the crack length, the specimen geometry and the applied loading, and (r,θ) are the cylindrical coordinates of a point with the origin located at the crack tip and the positive angle measured counterclockwise from the axis of the crack.

After using trigonometric identities, one can show that all of the functions in Eqs. (9) and (10) are spanned by the following four basis functions:

$$\left\{ \sqrt{r}\cos\frac{\theta}{2} \quad \sqrt{r}\sin\frac{\theta}{2} \quad \sqrt{r}\sin\frac{\theta}{2}\sin\theta \quad \sqrt{r}\cos\frac{\theta}{2}\sin\theta \right\} \tag{11}$$

In the application of the meshfree method to linear elastic fracture mechanics (LEFM) problems, it is advantageous to add these four basis functions in Eq. (11) into the basis functions so that the stress singularity can be captured without having a very fine nodal density around the crack tip. It was first used by Fleming et al. [12] in the element-free Galerkin (EFG) method and called the resulting basis as enriched basis functions.

Adding these four basis functions in Eq. (11) into Eq. (1), we can obtain the enriched basis functions for a two-dimensional problem:

(a) with complete linear monomials

$$\mathbf{p}^{\mathrm{T}}(\mathbf{x}) = \left[1, x, y, \sqrt{r}\cos\frac{\theta}{2}, \sqrt{r}\sin\frac{\theta}{2}, \sqrt{r}\sin\frac{\theta}{2}\sin\theta, \sqrt{r}\cos\frac{\theta}{2}\sin\theta\right] \tag{12}$$

(b) with complete second-order monomials

$$\mathbf{p}^{\mathrm{T}}(\mathbf{x}) = \left[1, x, y, x^2, xy, y^2, \sqrt{r}\cos\frac{\theta}{2}, \sqrt{r}\sin\frac{\theta}{2}, \sqrt{r}\sin\frac{\theta}{2}\sin\theta, \sqrt{r}\cos\frac{\theta}{2}\sin\theta\right] \tag{13}$$

3. Discrete equations of FEM and the meshfree method

Consider the following two-dimensional problem of solid mechanics in domain Ω bounded by Γ:

$$\nabla\sigma + \mathbf{b} = 0 \quad \text{in } \Omega \tag{14}$$

where σ is the stress tensor, which corresponds to the displacement field $\mathbf{u} = \{u, v\}^{\mathrm{T}}$, $\mathbf{b}$ is the body force vector, and ∇ is the divergence operator. The boundary conditions are given as follows:

$$\mathbf{u} = \bar{\mathbf{u}} \quad \text{on } \Gamma_{\mathrm{u}} \tag{15}$$

$$\sigma \cdot \mathbf{n} = \bar{\mathbf{t}} \quad \text{on } \Gamma_{\mathrm{t}} \tag{16}$$

in which the superposed bar denotes prescribed boundary values and $\mathbf{n}$ is the unit outward normal to domain Ω.

The principle of minimum potential energy can be stated as follows: The solution of a problem in the small displacement theory of elasticity is the vector function $\mathbf{u}$ of displacement which minimizes the total potential energy Π given by

$$\Pi = \int_{\Omega} \frac{1}{2}\varepsilon^{\mathrm{T}} \cdot \sigma \mathrm{d}\Omega - \int_{\Omega} \mathbf{u}^{\mathrm{T}} \cdot \mathbf{b}\mathrm{d}\Omega - \int_{\Gamma_{\mathrm{t}}} \mathbf{u}^{\mathrm{T}} \cdot \bar{\mathbf{t}}\mathrm{d}\Gamma \tag{17}$$

with the boundary condition described in Eq. (15), where ε is the strain.

The meshfree method and FEM use the similar global weak form given in Eq. (17). The meshfree shape functions have been given in Section 2, and the interpolation formulation of FEM can be written as [22]

$$u = \sum_{i=1}^{n_{\mathrm{e}}} N_i(x) u_i \quad n_{\mathrm{e}} = 3, 4, 5, \ldots \tag{18}$$

where n_{e} is the number of nodes in a FE element, and N is the FE shape function.

Substituting the expression of $\mathbf{u}$ given in Eqs. (5) and (18), and using the stationary condition for Eq. (17) yield

$$\mathbf{K}_{(\mathrm{FE})}\mathbf{U}_{(\mathrm{FE})} = \mathbf{F}_{(\mathrm{FE})} \tag{19}$$

$$\mathbf{K}_{(\mathrm{MM})}\mathbf{U}_{(\mathrm{MM})} = \mathbf{F}_{(\mathrm{MM})} \tag{20}$$

where $\mathbf{K}_{(\mathrm{FE})}$, $\mathbf{U}_{(\mathrm{FE})}$, $\mathbf{F}_{(\mathrm{FE})}$, $\mathbf{K}_{(\mathrm{MM})}$, $\mathbf{U}_{(\mathrm{MM})}$, and $\mathbf{F}_{(\mathrm{MM})}$ are stiffness matrices, the displacement vectors, and the force vectors for FEM and the meshfree method, respectively. Now, we have

$$\mathbf{K}_{(\mathrm{FE})ij} = \int_{\Omega} \mathbf{B}^{\mathrm{T}}_{(\mathrm{FE})i} \mathbf{D} \mathbf{B}_{(\mathrm{FE})j} \mathrm{d}\Omega \tag{21}$$

$$\mathbf{K}_{(\mathrm{MM})ij} = \int_{\Omega} \mathbf{B}^{\mathrm{T}}_{(\mathrm{MM})i} \mathbf{D} \mathbf{B}_{(\mathrm{MM})j} \mathrm{d}\Omega \tag{22}$$

$$\mathbf{F}_{(\mathrm{FE})i} = \int_{\Gamma_{\mathrm{t}}} N_i \bar{\mathbf{t}} \mathrm{d}\Gamma + \int_{\Omega} N_i \mathbf{b} \mathrm{d}\Omega \tag{23}$$

$$\mathbf{F}_{(\mathrm{MM})i} = \int_{\Gamma_{\mathrm{t}}} \phi_i \bar{\mathbf{t}} \mathrm{d}\Gamma + \int_{\Omega} \phi_i \mathbf{b} \mathrm{d}\Omega \tag{24}$$

where $\mathbf{D}$ is the matrix of material constants, and

$$\mathbf{B}_{(\mathrm{FE})i} = \begin{bmatrix} N_{i,x} & 0 \\ 0 & N_{i,y} \\ N_{i,y} & N_{i,x} \end{bmatrix}, \quad \mathbf{B}_{(\mathrm{MM})i} = \begin{bmatrix} \phi_{i,x} & 0 \\ 0 & \phi_{i,y} \\ \phi_{i,y} & \phi_{i,x} \end{bmatrix} \tag{25}$$

4. Coupling of the meshfree method and FEM

4.1. Transition condition

As shown in Fig. 2, consider a two-dimensional problem domain with a crack. A sub-domain, $\Omega_{(\mathrm{MM})}$, including the crack is discretized by the meshfree nodes and the other sub-domain, $\Omega_{(\mathrm{FE})}$, uses FEM. These two domains are joined by a transition domain $\Omega_{(\mathrm{T})}$ that possesses displacement compatibility and force equilibrium in coupling $\Omega_{(\mathrm{MM})}$ and $\Omega_{(\mathrm{FEM})}$. This means that

$$\mathbf{u}_{(\mathrm{MM})k} = \mathbf{u}_{(\mathrm{FE})k} \tag{26}$$

$$\mathbf{f}_{(\mathrm{MM})k} + \mathbf{f}_{(\mathrm{FE})k} = 0 \tag{27}$$

where $\mathbf{u}_{(\mathrm{MM})k}$, $\mathbf{u}_{(\mathrm{FE})k}$, $\mathbf{f}_{(\mathrm{MM})k}$ and $\mathbf{f}_{(\mathrm{FE})k}$ are displacements and forces at a transition particle k obtained by the meshfree method in $\Omega_{(\mathrm{MM})}$ and FEM in $\Omega_{(\mathrm{FE})}$, respectively.

It will be ideal to satisfy both the displacement compatibility and the force equilibrium conditions, in which the displacement compatibility Eq. (26) is the most important and must be satisfied. In addition, because the meshfree MLSA shape functions lack the delta function properties, it is difficult to directly connect these two domains.

To satisfy the displacement compatibility condition, two combination techniques, using the hybrid displacement shape function algorithm [16] and the modified variational form algorithm [17], have been developed. However, in these techniques, as shown in Fig. 1, a common interface (a curve in the two-dimensional problem) is used between $\Omega_{(\mathrm{FE})}$ and $\Omega_{(\mathrm{MM})}$. The meshfree nodes and the FEM nodes along this interface coin-

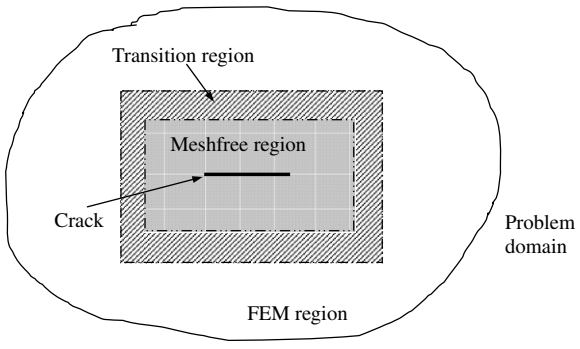

Fig. 2. The coupled analysis for the crack problem using the new transition technique.

cide with each other, and are dependent on each other. It will increase the computational cost and make difficulty for some problems. In addition, because only an interface curve is used, it is difficult to ensure the compatibility (especially the high-order continuity). In the following, we will develop a new transition technique to ensure a smooth transition between $\Omega_{(\mathrm{FE})}$ and $\Omega_{(\mathrm{MM})}$, which has been successfully used in the macro/micro/nano multiscale analysis [23].

4.2. Coupling technique

As shown in Fig. 2, there is a transition (or bridge) region, $\Omega_{(\mathrm{T})}$, between the FEM and meshfree domains. The generalized displacement of a point in the transition domain at $\mathbf{x}$ can be defined as

$$\mathbf{g} = \mathbf{u}_{(\mathrm{MM})}(\mathbf{x}) - \mathbf{u}_{(\mathrm{FE})}(\mathbf{x}) \tag{28}$$

where $\mathbf{u}_{(\mathrm{MM})}(\mathbf{x})$ and $\mathbf{u}_{(\mathrm{FE})}(\mathbf{x})$ are the displacements of a point $\mathbf{x}$, obtained by the interpolations using the meshfree nodes and the FEM element, respectively, i.e.,

$$\mathbf{u}_{(\mathrm{MM})}(\mathbf{x}) = \sum_I \mathbf{\Phi}_I(\mathbf{x})\mathbf{u}_{(\mathrm{MM})I} \tag{29}$$

$$\mathbf{u}_{(\mathrm{FE})}(\mathbf{x}) = \sum_J \mathbf{N}_J(\mathbf{x})\mathbf{u}_{(\mathrm{FE})J} \tag{30}$$

A sub-functional is introduced to enforce the displacement compatibility condition given in Eq. (26) by means of Lagrange multiplier λ in the transition domain

$$\begin{aligned} \Pi_{(\mathrm{T})} &= \int_{\Omega_{(\mathrm{T})}} \boldsymbol{\lambda}\cdot\mathbf{g}\,\mathrm{d}\Omega = \int_{\Omega_{(\mathrm{T})}} \boldsymbol{\lambda}\cdot\left[\mathbf{u}_{(\mathrm{MM})} - \mathbf{u}_{(\mathrm{FE})}\right]\mathrm{d}\Omega \\ &= \int_{\Omega_{(\mathrm{T})}} \boldsymbol{\lambda}\cdot\mathbf{u}_{(\mathrm{MM})}\,\mathrm{d}\Omega - \int_{\Omega_{(\mathrm{T})}} \boldsymbol{\lambda}\cdot\mathbf{u}_{(\mathrm{FE})}\,\mathrm{d}\Omega \\ &= \Pi^{(\mathrm{MM})}_{(\mathrm{T})} - \Pi^{(\mathrm{FE})}_{(\mathrm{T})} \end{aligned} \tag{31}$$

In which, $\Pi^{(\mathrm{MM})}_{(\mathrm{T})}$ and $\Pi^{(\mathrm{FE})}_{(\mathrm{T})}$ are the sub-functional for the meshfree part and the FEM part. Substituting $\Pi^{(\mathrm{MM})}_{(\mathrm{T})}$ and $\Pi^{(\mathrm{FE})}_{(\mathrm{T})}$ separately into Eq. (17) for the meshfree method and FEM, their generalized functional forms can be written as

$$\Pi_{(\mathrm{MM})} = \int_{\Omega_{(\mathrm{MM})}} \frac{1}{2}\boldsymbol{\varepsilon}^{\mathrm{T}}\cdot\boldsymbol{\sigma}\,\mathrm{d}\Omega - \int_{\Omega_{(\mathrm{MM})}} \mathbf{u}^{\mathrm{T}}\cdot\mathbf{b}\,\mathrm{d}\Omega - \int_{\Gamma_{(\mathrm{MM})^t}} \mathbf{u}^{\mathrm{T}}\cdot\bar{\mathbf{t}}\,\mathrm{d}\Gamma + \int_{\Omega_{(\mathrm{T})}} \boldsymbol{\lambda}\cdot\mathbf{u}_{(\mathrm{MM})}\,\mathrm{d}\Omega \tag{32}$$

$$\Pi_{(\mathrm{FE})} = \int_{\Omega_{(\mathrm{FE})}} \frac{1}{2}\boldsymbol{\varepsilon}^{\mathrm{T}}\cdot\boldsymbol{\sigma}\,\mathrm{d}\Omega - \int_{\Omega_{(\mathrm{FE})}} \mathbf{u}^{\mathrm{T}}\cdot\mathbf{b}\,\mathrm{d}\Omega - \int_{\Gamma_{(\mathrm{FE})^t}} \mathbf{u}^{\mathrm{T}}\cdot\bar{\mathbf{t}}\,\mathrm{d}\Gamma - \int_{\Omega_{(\mathrm{T})}} \boldsymbol{\lambda}\cdot\mathbf{u}_{(\mathrm{FE})}\,\mathrm{d}\Omega \tag{33}$$

In these variational formulations, the domains of $\Omega_{(\mathrm{FE})}$ and $\Omega_{(\mathrm{MM})}$ are connected via Lagrange multiplier λ, which can be given by the interpolation functions Λ and the nodal value of λ_i

$$\boldsymbol{\lambda} = \sum_i \Lambda_i\cdot\boldsymbol{\lambda}_i \tag{34}$$

Λ is the selected interpolation for λ_i and it can be the FEM shape function.

Substituting Eqs. (5) and (34) into Eq. (32), and using the stationary condition based on the displacement, the following meshfree equations can be obtained

$$\begin{bmatrix}\mathbf{K}_{(\mathrm{MM})} & \mathbf{B}_{(\mathrm{MM})}\end{bmatrix}\begin{Bmatrix}\mathbf{U}_{(\mathrm{MM})} \\ \boldsymbol{\lambda}\end{Bmatrix} = \left\{\mathbf{F}_{(\mathrm{MM})}\right\} \tag{35}$$

where $\mathbf{K}_{(\mathrm{MM})}$ and $\mathbf{F}_{(\mathrm{MM})}$ have been defined in Eqs. (22) and (24), $\mathbf{B}_{(\mathrm{MM})}$ is defined as

$$\mathbf{B}_{(\mathrm{MM})} = \int_{\Omega_{(\mathrm{T})}} \mathbf{\Lambda}\mathbf{\Phi}^{\mathrm{T}}\,\mathrm{d}\Omega \tag{36}$$

Substituting Eqs. (18) and (34) into Eq. (33), and using the stationary condition based on the displacement, lead to the following FEM equations

$$\begin{bmatrix}\mathbf{K}_{(\mathrm{FE})} & -\mathbf{B}_{(\mathrm{FE})}\end{bmatrix}\begin{Bmatrix}\mathbf{U}_{(\mathrm{FE})}\\ \boldsymbol{\lambda}\end{Bmatrix} = \{\mathbf{F}_{(\mathrm{FE})}\} \tag{37}$$

where $\mathbf{K}_{(\mathrm{FE})}$ and $\mathbf{F}_{(\mathrm{FE})}$ have been defined in Eqs. (21) and (23), $\mathbf{B}_{(\mathrm{FE})}$ is defined as

$$\mathbf{B}_{(\mathrm{FE})} = \int_{\Omega_{(\mathrm{T})}} \boldsymbol{\Lambda} N^{\mathrm{T}} \mathrm{d}\Omega \tag{38}$$

It should be mentioned here that it is impossible to solve Eqs. (35) and (37) separately. To obtain the unique solution for the global problem, using the stationary condition of Eqs. (35) and (37) based on the Lagrange multiplier and considering the compatibility condition, we can obtain the following relationship,

$$\mathbf{B}^{\mathrm{T}}_{(\mathrm{MM})}\mathbf{U}_{(\mathrm{MM})} - \mathbf{B}^{\mathrm{T}}_{(\mathrm{FE})}\mathbf{U}_{(\mathrm{FE})} = \mathbf{0} \tag{39}$$

Because the meshfree and FEM domains are connected through the transition domain, the assembly of Eqs. (35), (37) and (39) yields a linear system of the following form

$$\begin{bmatrix}\mathbf{K}_{(\mathrm{MM})} & \mathbf{0} & \mathbf{B}_{(\mathrm{MM})}\\ \mathbf{0} & \mathbf{K}_{(\mathrm{FE})} & -\mathbf{B}_{(\mathrm{FE})}\\ \mathbf{B}^{\mathrm{T}}_{(\mathrm{MM})} & -\mathbf{B}^{\mathrm{T}}_{(\mathrm{FE})} & \mathbf{0}\end{bmatrix}\begin{Bmatrix}\mathbf{U}_{(\mathrm{MM})}\\ \mathbf{U}_{(\mathrm{FE})}\\ \boldsymbol{\lambda}\end{Bmatrix} = \begin{Bmatrix}\mathbf{F}_{(\mathrm{MM})}\\ \mathbf{F}_{(\mathrm{FE})}\\ \mathbf{0}\end{Bmatrix} \tag{40}$$

Solving Eq. (40) together with the displacement boundary condition, given in Eq. (15), we can obtain the solution for the problem considered.

To satisfy the force equilibrium condition, the generalized derivative at a point $\mathbf{x}$ can be written as

$$\mathbf{g}_{(x)} = \frac{\partial \mathbf{u}_{(\mathrm{MM})}(\mathbf{x})}{\partial \mathbf{x}} - \frac{\partial \mathbf{u}_{(\mathrm{FE})}(\mathbf{x})}{\partial \mathbf{x}} \tag{41}$$

Using Lagrange multiplier γ, we have

$$\begin{aligned}\Pi_{(\mathrm{T})(\mathbf{x})} &= \int_{\Omega_{(\mathrm{T})}} \boldsymbol{\gamma}\cdot\mathbf{g}\mathrm{d}\Omega\\ &= \int_{\Omega_{(\mathrm{T})}} \boldsymbol{\gamma}\cdot\frac{\partial \mathbf{u}_{(\mathrm{MM})}(\mathbf{x})}{\partial \mathbf{x}}\mathrm{d}\Omega - \int_{\Omega_{(\mathrm{T})}} \boldsymbol{\gamma}\cdot\frac{\partial \mathbf{u}_{(\mathrm{FE})}(\mathbf{x})}{\partial \mathbf{x}}\mathrm{d}\Omega\\ &= \Pi^{(\mathrm{MM})}_{(\mathrm{T})(\mathbf{x})} - \Pi^{(\mathrm{FE})}_{(\mathrm{T})(\mathbf{x})}\end{aligned} \tag{42}$$

Following the similar procedure from Eqs. (32)–(40), we can obtain the coupling equations to satisfy the high-order continuity

$$\begin{bmatrix}\mathbf{K}_{(\mathrm{MM})} & \mathbf{0} & \mathbf{B}_{(\mathrm{MM})} & \mathbf{A}_{(\mathrm{MM})}\\ \mathbf{0} & \mathbf{K}_{(\mathrm{FE})} & -\mathbf{B}_{(\mathrm{FE})} & -\mathbf{A}_{(\mathrm{FE})}\\ \mathbf{B}^{\mathrm{T}}_{(\mathrm{MM})} & -\mathbf{B}^{\mathrm{T}}_{(\mathrm{FE})} & \mathbf{0} & \mathbf{0}\\ \mathbf{A}^{\mathrm{T}}_{(\mathrm{MM})} & -\mathbf{A}^{\mathrm{T}}_{(\mathrm{FE})} & \mathbf{0} & \mathbf{0}\end{bmatrix}\begin{Bmatrix}\mathbf{U}_{(\mathrm{MM})}\\ \mathbf{U}_{(\mathrm{FE})}\\ \boldsymbol{\lambda}\\ \boldsymbol{\gamma}\end{Bmatrix} = \begin{Bmatrix}\mathbf{F}_{(\mathrm{MM})}\\ \mathbf{F}_{(\mathrm{FE})}\\ \mathbf{0}\\ \mathbf{0}\end{Bmatrix} \tag{43}$$

where

$$\mathbf{A}_{(\mathrm{MM})} = \int_{\Omega_{(\mathrm{T})}} \Psi\frac{\partial \boldsymbol{\Phi}^{\mathrm{T}}}{\partial \mathbf{x}}\mathrm{d}\Omega \tag{44}$$

$$\mathbf{A}_{(\mathrm{FE})} = \int_{\Omega_{(\mathrm{T})}} \Psi\frac{\partial \mathbf{N}^{\mathrm{T}}}{\partial \mathbf{x}}\mathrm{d}\Omega \tag{45}$$

In which Ψ are the interpolation functions for γ.

4.3. Numerical implementations

(a) *The size of transition region.* The size of transition region will affect the performance of the coupled method. If the size is too small, it will decrease the accuracy of the transition, especially for the high-order compatibility. If the size is too big, it will significantly increase the computational cost. For many problems, it is reasonable to use the following size of transition region:

$$h_t \cong (3 \sim 5) \cdot d_{\mathrm{FE}} \text{ or } (3 \sim 5) \cdot d_{\mathrm{MM}} \tag{46}$$

where d_{FE} and d_{MM} are equivalent sizes of FEM element and meshfree nodal space.

(b) *The transition particles.* To get $\mathbf{B}_{(\mathrm{MM})}$ and $\mathbf{B}_{(\mathrm{FEM})}$ numerically, the transition region can be divided into regular background cells, which are similar to those used in the meshfree method. However, these cells are totally independent of the FE elements and the meshfree background cells. In the practical computation, to simplify the integration and reduce the ''meshing'' cost, several layers of transition particles, which are regularly distributed, can be inserted in the transition domain $\Omega_{(\mathrm{T})}$. The displacement compatibility between FEM and meshfree nodes is achieved through these transition particles. The advantages of using these transition particles are clear. First, they allow the meshfree nodes in $\Omega_{(\mathrm{MM})}$ to have an arbitrary distribution and become independent of the distributions of the FEM nodes in $\Omega_{(\mathrm{FE})}$. Second, the compatibility conditions in the transition domain can be conveniently controlled through the adjustment of the number and distribution of the transition particles. For some sub-transition domains with stronger compatibility requirement, a finer transition particle distribution can be arranged. Third, the compatibility of higher order derivatives can be easily satisfied.

(c) *Lagrange multipliers*. The above Lagrange multiplier method is accurate and the physical meaning is also very clear. However, it will increase the computational cost (especially when the number of transition particles is large) because new variables (Lagrange multipliers) are added. Hence, we can use the constant Lagrange multipliers to yield the so-called penalty method, i.e., the common Lagrange multiplier method can be used to obtain a range of penalty coefficients, and then use them as constants for this problem and other similar problems to improve computational efficiency.

5. The relay model

With the use of node based interpolation techniques, meshfree methods offer great opportunities to handle problems of complex geometry including cracks. However, there is general discontinuity of displacements across a crack, and the interpolation domain used for the construction of meshfree shape functions can contain numerous irregular boundary fragments and the computation of nodal weights based on physical distance can be erroneous. This issue will become more serious in dealing with the fracture problems, especially for the multi-cracking problems. Several techniques have been reported on the construction of meshfree approximations with discontinuities and non-convex boundaries, including the visibility method [2], the diffraction method [24], and the transparency method [24]. However, these methods are only effective for problems with relatively simple domains (e.g., with one or two cracks, or not many non-convex portions on the boundaries), but not effective for domains with highly irregular boundaries (e.g., with many cracks). Liu and Tu [25] have developed a relay model to determine the domain of influence of a node in a complex problem domain.

The relay model is motivated by the way of a radio communication system composed of networks of relay stations. Consider an interpolation domain containing a large number of irregular boundary fragments (or cracks) as shown in Fig. 3, in which O is the interpolation point, P is the field node, and R is the relay point. The field node, e.g., P_2, first radiates its influence in all directions equally, liking a radio signal being broadcasted at a radio station, until the contained boundaries are encountered. Then its' influence is relayed through relay points, e.g., $R_{2\text{-}1}$ and $R_{1\text{-}1}$, to reach the interpolation point O. The distance (called equivalent distance) between the interpolation point and the field node can then be calculated. In addition, the weight parameter used in MLSA is measured by the equivalent distance that can be computed based on the relay region defined by a circle involute. The details for the relay model can be found in Liu [20] and Liu and Tu [25].

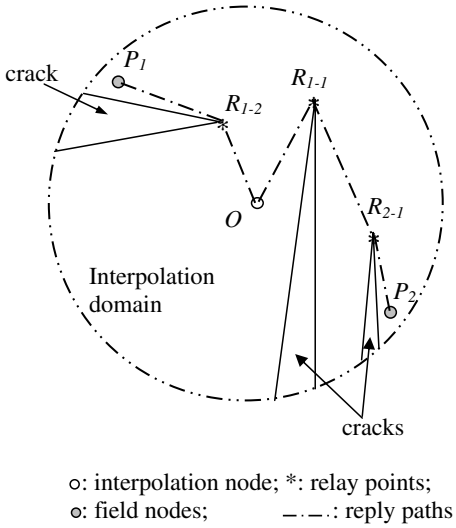

Fig. 3. Relay model for an irregular domain with discontinuous boundaries.

6. Numerical results and discussions

Several cases of two-dimensional fracture problems have been studied in order to examine the present coupled MM/FE method. Except when mentioned, the units are taken as standard international (SI) units in the following examples.

6.1. Cantilever beam

The coupled method is first verified by a two-dimensional cantilever beam problem, because its' analytical solution is available and can be found in textbooks, e.g., Timoshenko and Goodier [26]. Consider a beam, as shown in Fig. 4a, with length L and height D subjected to a parabolic traction at the free end. The parameters

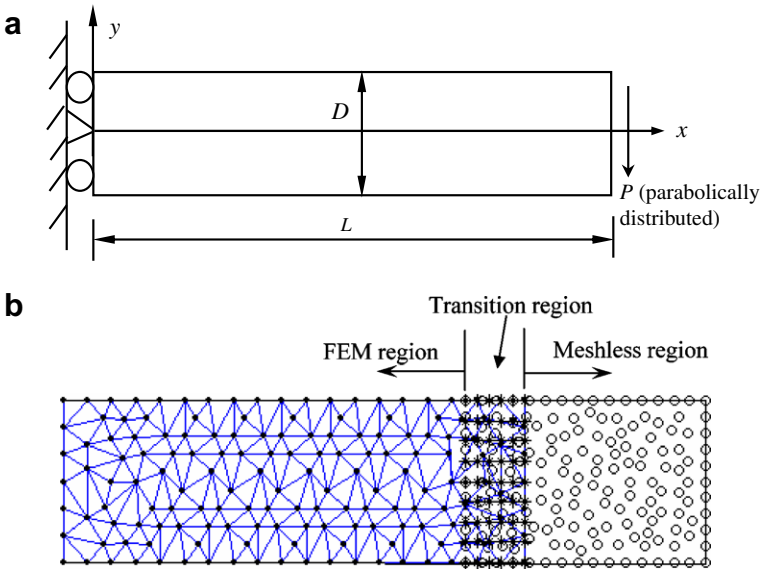

Fig. 4. (a) A cantilever beam subjected to a parabolic traction at the free end and (b) the computational model for the two-dimensional cantilever beam.

of the beam are taken as $E = 3.0 \times 10^7$, $v = 0.3$, $D = 12$, $L = 48$, and $P = 1000$. The beam has a unit thickness and a plane stress problem is considered.

As shown in Fig. 4b, the beam is divided into two parts. FEM using the triangular elements is used in the left part where the essential boundary condition is included. The meshfree method is used in the right part where the traction boundary condition is included. These two parts are connected through a transition region that is discretized by 54 regularly distributed transition particles. Fig. 5 illustrates the comparison between the shear stress calculated analytically and by the coupled method at the cross-section of $x = L/2$, which shows an excellent agreement between the analytical and numerical results.

6.2. Near-tip crack field

A well-known near-tip field, which is subjected to a mode-I displacement field at its edges, is analyzed. As shown in Fig. 6, an edge-cracked square plate is subjected to the following displacement field for a model-I crack [1].

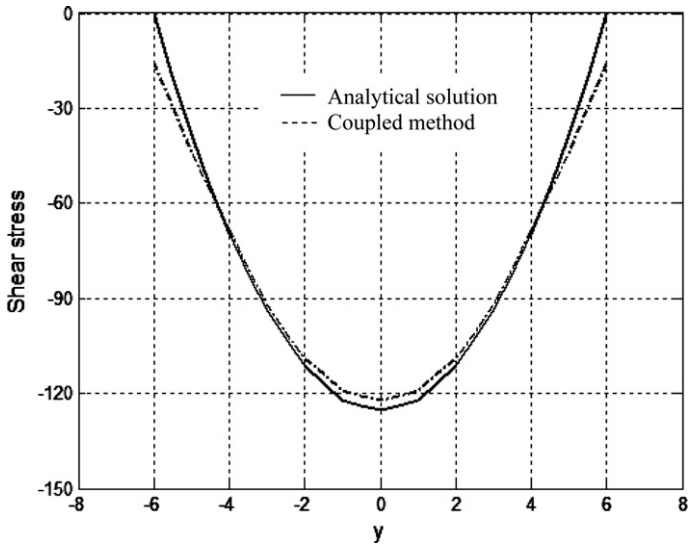

Fig. 5. Shear stress distributions on the cross-section of the beam at $x = L/2$.

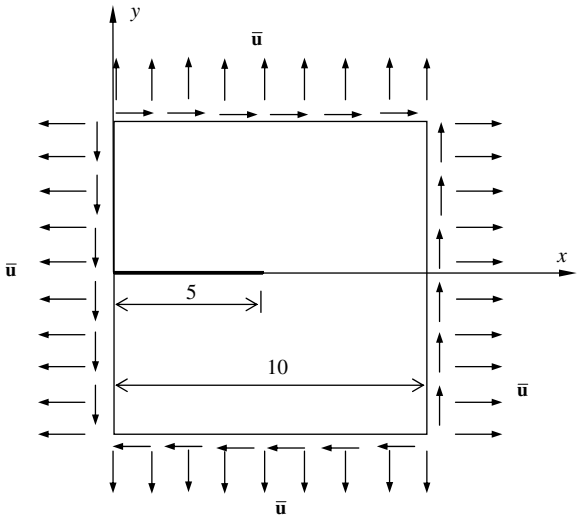

Fig. 6. A cracked square plate subjected to mode-I displacement boundary conditions.

$$\begin{Bmatrix} u \\ v \end{Bmatrix} = \frac{K_I}{2\mu}\sqrt{\frac{r}{2\pi}}\begin{Bmatrix} \cos\frac{\theta}{2}\left[k-1+2\sin^2\frac{\theta}{2}\right] \\ \sin\frac{\theta}{2}\left[k+1-2\cos^2\frac{\theta}{2}\right] \end{Bmatrix} \tag{47}$$

where k is the Kolosov constant.

Hence, the analytical solution for the stress field is given in Eq. (9).

The plate is divided into two parts: the meshfree method is used for the central part, in which the crack embedded, and FEM is used for other parts. The computational model is plotted in Fig. 7: 441 irregularly distributed nodes are used in the meshfree domain, 578 triangular FEM elements are used in the FEM domain, and 210 regularly distributed transition particles are used in the transition domains. Fig. 8 shows the stress distribution along the crack axis (when $\theta = 0°$). Clearly, the prediction of the new developed method matches the analytical solution very well.

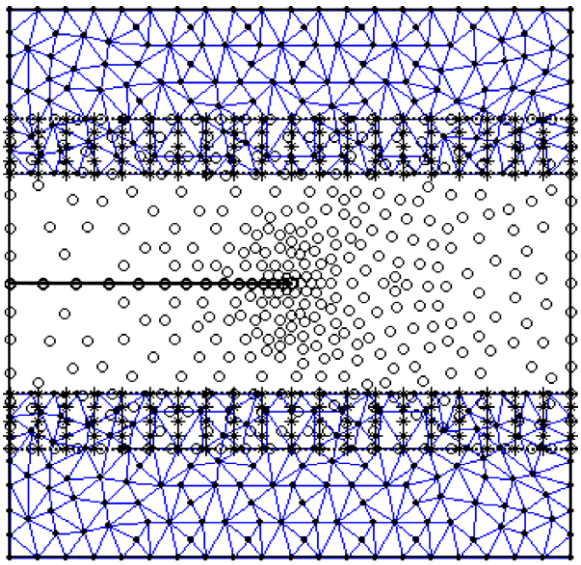

Fig. 7. The computational model for the edge-cracked plate.

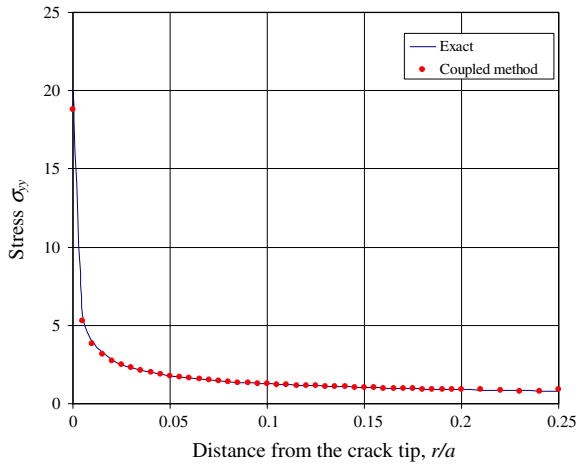

Fig. 8. The distribution of σ_{yy} along the axis of the crack ($\theta = 0$).

It should be mentioned that the sole FEM will lead to worse accuracy for this problem, especially for the stress distributions around the crack tip, because FEM without the enriched basis function usually has bad accuracy and is difficult to capture the stress singularity near the crack tip. Although using the high-order FEM elements can partly solve this issue, FEM still has technical difficulty for the fracture problems (especially the dynamic fracture problems). It has also been proven [12] that the sole meshfree method has much better accuracy for the crack problem. However, the computational efficiency will be worse if the sole meshfree method is used. Our studies show that the present coupled method can keep the good accuracy of the meshfree method for the crack tip field, and, at the same time, it can save much computational cost because of the use of FEM in the regions far away from the crack tip.

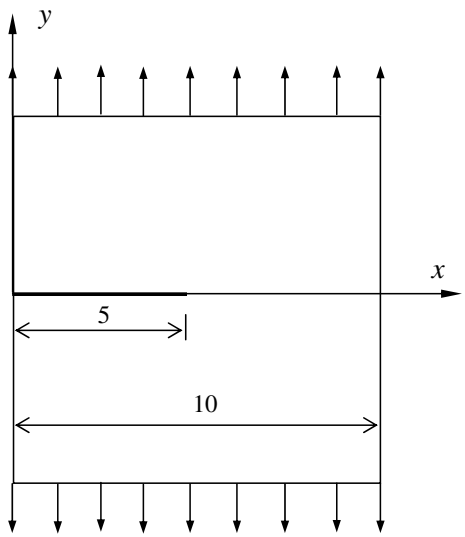

Fig. 9. An edge square plate subjected to the tension loading.

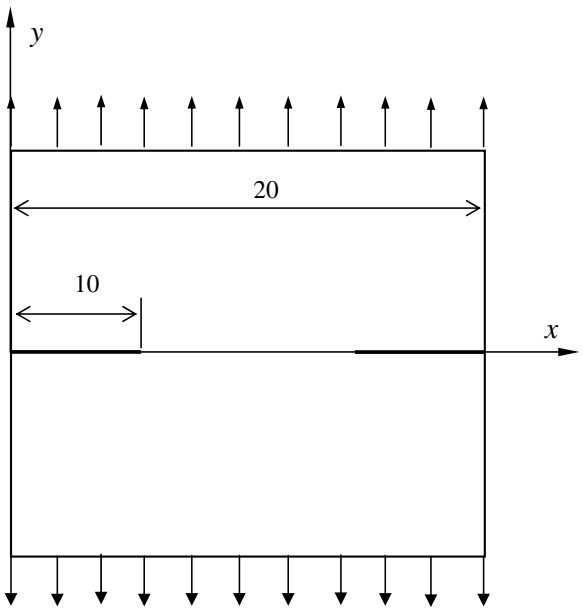

Fig. 10. A double-edge square plate subjected to the tension loading.

6.3. Two edge-cracked plates loaded in tension

An edge-cracked square plate subjected to a uniformed tension of $f = 1.0$, as shown in Fig. 9, is studied. The plane strain case is considered, and $E = 1000$, $v = 0.25$. The analytical results for K_I had been given by Gdoutos [28] and Ching and Batra [27]. For these parameters used here, the analytical $(K_I)_{analytical} = 11.2$.

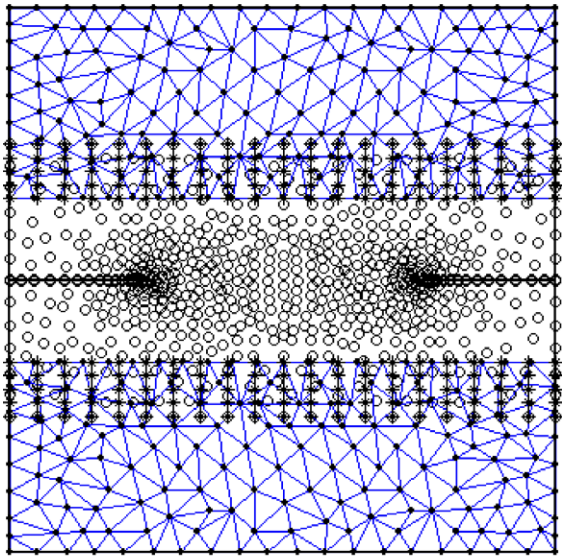

Fig. 11. The computational model for the plate with two edge cracks.

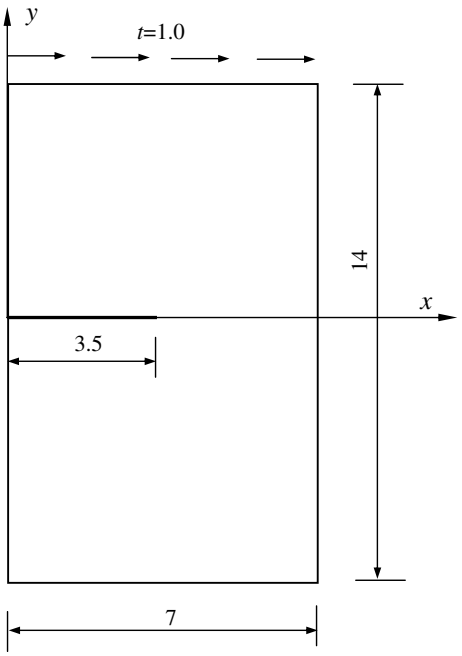

Fig. 12. An edge-cracked plate subjected to the shear loading.

The computational model is the same as that used in Section 6.2 and shown in Fig. 7. Stress intensity factors were computed using the domain form of the J-integral. Our study found that the coupled method using the MLSA with the enriched basis functions makes the J-integral almost domain independent, given to $(K_I)_{numerical} = 11.31$. Compared with the analytical solution, the coupled method leads to a stable and accurate result.

A square plate with double edge cracks shown in Fig. 10 is also studied. The computational model in Fig. 11 contains 705 irregularly distributed nodes in the meshfree domain, 538 triangular FEM elements in the FEM domain, and 210 regularly distributed transition particles in the transition domains. Ching and Batra [27] studied the same problem and the analytical K_I given by Gdouos [28] is $(K_I)_{analytical} = 4.65$.

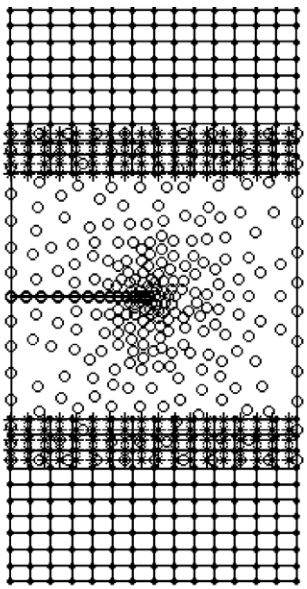

• FEM nodes; o meshless nodes; * transition particles

Fig. 13. The computational model for the edge-cracked plate subjected to the shear loading.

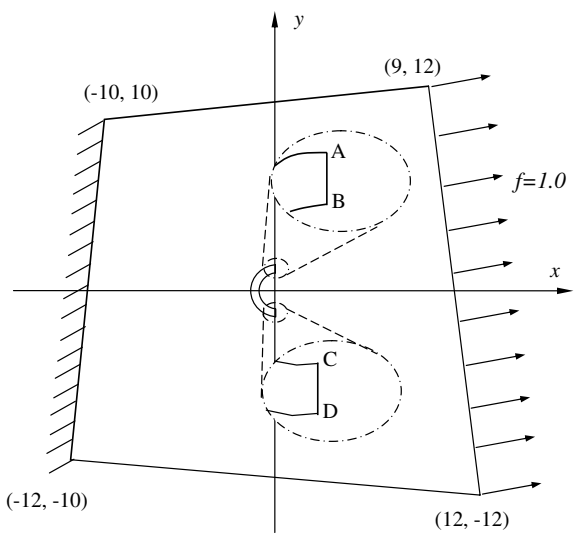

Fig. 14. A plate with a "C" shaped center crack.

Using the J-integral, the present coupled method gives $(K_I)_{numerical} = 4.75$. The coupled method leads to a very accurate result.

6.4. Shear edge crack

In this example, a clamped plate with an edged crack and subjected to shear traction is considered. The parameters have been shown in Fig. 12. The material constants used are $E = 3.0 \times 10^6$ units and $\upsilon = 0.25$. A plane strain state of deformation is assumed. The reference solution for the stress intensity factors has been given by Fleming et al. ([12]) and Ching and Batra [27] with $K_I = 34$ and $K_{II} = 4.55$. Our computational model in Fig. 13 has 284 irregularly distributed nodes in the meshfree domain, 280 bi-linear FEM elements in the FEM domain, and 180 regularly distributed transition particles in the transition domains. The present coupled method works well for this problem and the computational errors are less than 2% for both K_I and K_{II}.

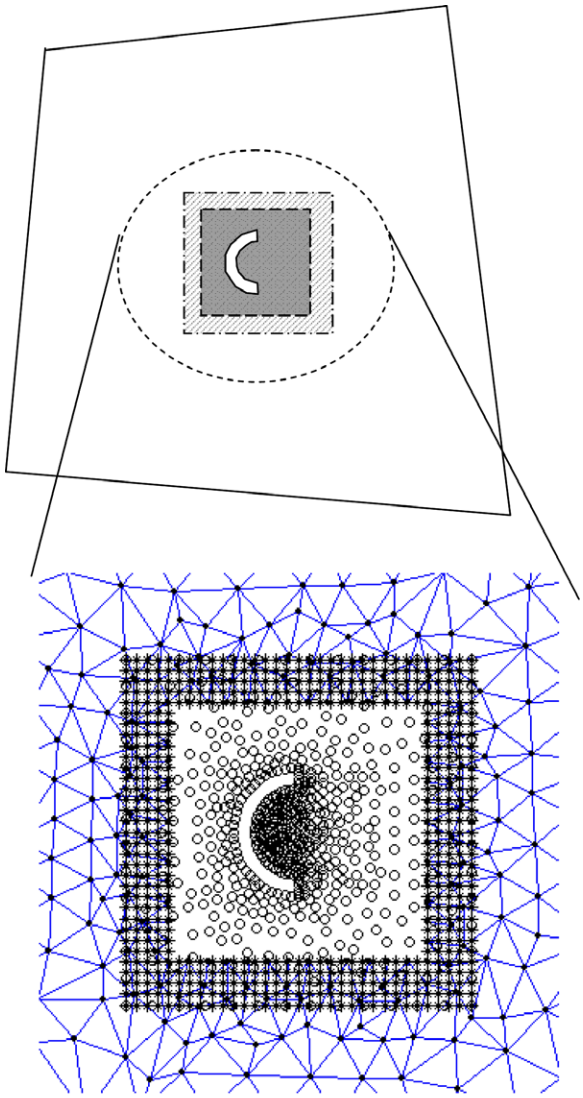

• FEM nodes; o meshless nodes; * transition particles

Fig. 15. The computational model for the plate with the "C" shaped center crack.

6.5. Cracks in a complex shaped plate

Let us now consider a plate of complex shape with a "C" shaped crack. The material constants used are $E = 3.0 \times 10^7$ and $\upsilon = 0.3$. One edge of the plate is fixed, one edge is subjected to uniformly distributed tension load, and the rest edges are traction free. As shown in Fig. 14, the plate is divided into two parts. The meshfree method is used in the central part including the crack, and FEM is used for other parts. The computational model shown in Fig. 15 contains 595 irregularly distributed nodes in the meshfree domain, 660 triangular FEM elements in the FEM domain, and 560 regularly distributed transition particles in the transition domains. As a reference solution, this problem is also analyzed by the sole meshfree method (the software of MFree 2D: Liu [20]) with very fine nodal distribution. Fig. 16 shows the distribution of stress, σ_{xx}, obtained by the present coupled method. It is almost identical with the meshfree method result. Table 1 lists the comparison of displacements and stress of four points shown in Fig. 14.

Fig. 17 shows the stress distribution along y-axis, and, again, very good agreement is obtained between the coupled method and the purely meshfree method. The stress concentrations on the crack tips have been clearly shown with the stress concentration factor around 3.3.

It should be mentioned here that for this problem, the coupled method uses less computational cost than the pure meshfree method, because we only apply the meshfree method in a very small region (about 10% of the problem domain) and FEM is used in the other area when FEM has a better computational efficiency than the meshfree method (Liu and Gu [13]). Hence, the advantage of the present coupled method has been proven by this example.

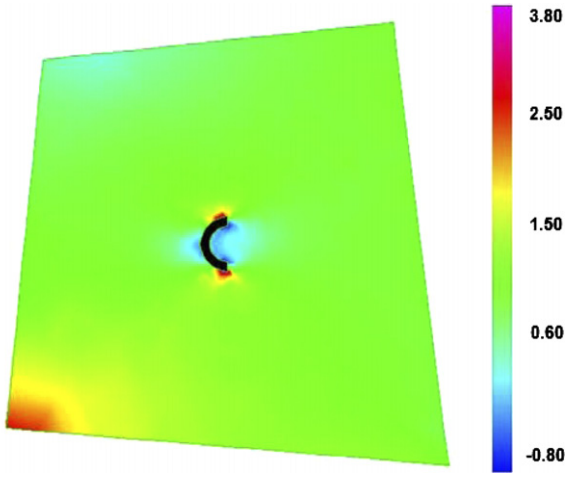

Fig. 16. The distribution of σ_{xx}.

Table 1
The displacements and stresses for four points in this plate

		Displacement		Stress		
		u ($\times 10^{-7}$)	v ($\times 10^{-7}$)	σ_{xx}	σ_{yy}	τ_{xy}
Point A	MFree 2D	4.1	3.4	2.31	−0.02	−0.03
	The coupled method	3.9	3.2	2.27	−0.017	−0.028
Point B	MFree 2D	4.9	2.8	−0.57	−1.6	−0.45
	The coupled method	4.7	2.9	−0.61	−1.72	−0.55
Point C	MFree 2D	5.3	4.2	−0.56	−1.05	0.36
	The coupled method	5.2	4.0	−0.54	−1.01	0.32
Point D	MFree 2D	4.5	4.3	3.51	1.13	1.37
	The coupled method	4.2	4.2	3.34	1.08	1.32

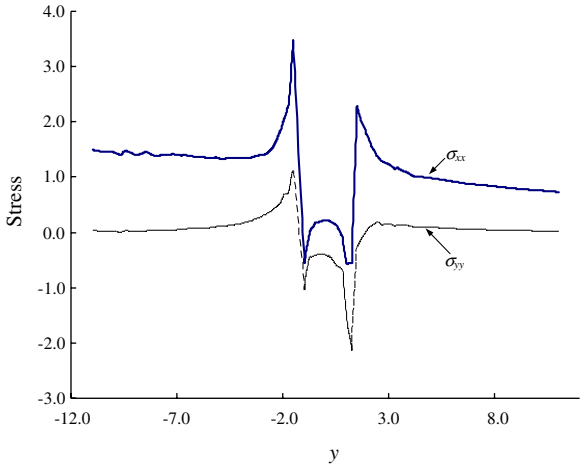

Fig. 17. The distribution of σ_{xx} and σ_{yy} along the y-axis.

7. Concluding remarks

FEM often has experiences difficulties in fracture mechanics problems because of difficulty in the re-meshing. Meshfree methods are effective for these crack problems, but they usually have worse computational efficiency. In the analysis of crack problems, we can find that a crack region usually occupies only a small part in the whole problem domain. It is desirable and beneficial to combine the meshfree methods with FEM in order to exploit their advantages while evading their disadvantages.

A novel coupled meshfree/FEM method has been developed in this paper for the analysis of crack problems. In this coupled method, the meshfree method is used only in a sub-domain including the crack and FEM is employed in the remaining part. Several numerical techniques are developed to ensure the effectiveness for this coupled method, including:

(a) The transition particles are inserted in the transition domain. Through these particles, a Lagrange multiplier method is used to ensure the compatibility of displacements and their gradients in the transition.
(b) The relay model is used for the effective construction of meshfree interpolation domains considering the discontinuous boundaries.

Numerical examples have been studied to demonstrate effectiveness of the present coupled method for crack problems, and very goods results have been obtained. The coupled method holds the advantages of both the FEM and meshfree methods including: (1) a lower computation cost; (2) a good accuracy; (3) the enhanced compatibility in the transition domain between the FEM domain and meshfree domain. Hence, it has been proven that the new coupled method is effective and robust for the analysis of fracture mechanics problems, and it has very good potential to become a powerful numerical tool.

Acknowledgement

This work was supported by an ARC Discovery Grant.

References

[1] Gingold RA, Moraghan JJ. Smooth particle hydrodynamics: theory and applications to non-spherical stars. Mon Not R Astron Soc 1977;181:375–89.
[2] Belytschko T, Lu YY, Gu L. Element-free Galerkin methods. Int J Numer Meth Engng 1994;37:229–56.
[3] Liu WK, Jun S, Zhang Y. Reproducing kernel particle methods. Int J Numer Meth Engng 1995;20:1081–106.

[4] Liew KM, Wu YC, Zou GP, Ng TY. Elasto-plasticity revisited: numerical analysis via reproducing kernel particle method and parametric quadratic programming. Int J Numer Meth Engng 2002;55:669–83.
[5] Atluri SN, Shen SP. The meshfree local Petrov–Galerkin (MLPG) method. Tech Science Press. Encino, USA, 2002.
[6] Atluri SN, Zhu T. A new meshfree local Petrov–Galerkin (MLPG) approach in computational mechanics. Computational Mechanics 1998;22:117–27.
[7] Gu YT, Liu GR. A meshfree local Petrov–Galerkin (MLPG) method for free and forced vibration analyses for solids. Comput Mech 2001;27(3):188–98.
[8] Gu YT, Liu GR. A local point interpolation method for static and dynamic analysis of thin beams. Comput Method Appl M 2001;190:5515–28.
[9] Liu GR, Gu YT. A local radial point interpolation method (LR-PIM) for free vibration analyses of 2-D solids. J Sound Vib 2001;246(1):29–46.
[10] Wang QX, Lam KY, et al. Analysis of microelectromechanical systems (MEMS) by meshless local Kriging (LoKriging) method. J Chinese Inst Engineers 2003;27(4):573–83.
[11] Liew KM, Chen XL. Mesh-free radial point interpolation method for the buckling analysis of Mindlin plates subjected to in-plane point loads. Int J Numer Meth Engng 2004;60(11):1861–77.
[12] Fleming M, Chu Y, Moran B, Belytschko T. Enriched element-free Galerkin methods for crack tip fields. Int J Numer Meth Engng 1997;40:1483–504.
[13] Liu GR, Gu YT. An introduction to meshfree methods and their programming. Berlin: Springer; 2005.
[14] Belytschko T, Organ D. Coupled finite element–element-free Galerkin method. Comput Mech 1995;17:186–95.
[15] Hegen D. Element-free Galerkin methods in combination with finite element approaches. Comput Meth Appl Mech. Engng 1996;135:143–66.
[16] Gu YT, Liu GR. A coupled element free Galerkin/boundary element method for stress analysis of two-dimensional solids. Comput Meth Appl Mech. Engng 2001;190/34:4405–19.
[17] Gu YT, Liu GR. Hybrid boundary point interpolation methods and their coupling with the element free Galerkin method. Engng Anal Bound Elem 2003;27(9):905–17.
[18] Liu GR, Gu YT. Meshfree local Petrov–Galerkin (MLPG) method in combination with finite element and boundary element approaches. Comput Mech 2000;26(6):536–46.
[19] Gu YT, Liu GR. Meshfree methods coupled with other methods for solids and structures. Tsinghua Science and Technology 2005;10(1):8–15.
[20] Liu GR. Mesh free methods: moving beyond the finite element method. USA: CRC Press; 2002.
[21] Anderson TL. Fracture mechanics: fundamental and applications. 1st ed. CRC Press; 1991.
[22] Zienkiewicz OC, Taylor RL. The finite element method. 5th ed. Oxford, UK: Butterworth Heinemann; 2000.
[23] Gu YT, Zhang LC. A concurrent multiscale method for structures based on the combination of the meshfree method and the molecular dynamics. Multiscale Modeling and Simulation: A SIAM Interdisciplinary Journal 2006;5(4):1128–55.
[24] Organ DJ, Fleming M, Belytschko T. Continuous meshfree approximations for nonconvex bodies by diffraction and transparency. Comput Mech 1996;18:225–35.
[25] Liu GR, Tu ZH. An adaptive procedure based on background cells for meshfree methods. Comput Meth Appl Mech Engng 2002;191:1923–43.
[26] Timoshenko SP, Goodier JN. Theory of elasticity. 3rd ed. New York: McGraw-hill; 1970.
[27] Ching HK, Batra RC. Determination of crack tip fields in linear elastostatics by the meshfree local Petrov–Galerkin (MLPG) method. CMES 2001;l2(2):273–89.
[28] Gdoutos EE. Fracture mechanics: an introduction. Kluwer Academic Publishers; 1993.